

Holographic non-relativistic fermionic fixed point and bulk dipole coupling

Wei-Jia Li

Department of Physics, Beijing Normal University, 100875 Beijing, China

wjli@mail.bnu.edu.cn

Hongbao Zhang

Crete Center for Theoretical Physics, Department of Physics,

University of Crete, 71003 Heraklion, Greece

hzhang@physics.uoc.gr

ABSTRACT: Inspired by the recently discovered non-relativistic fermionic fixed points, we investigate how the presence of bulk dipole coupling modifies the spectral function at one of these novel fixed points. As a result, although the infinite flat band is always visible in the presence of the bulk dipole coupling as well as chemical potential, the band is modified in a remarkable way at small momenta up to the order of magnitude of bulk dipole coupling. On the other hand, like a phoenix, a new Fermi surface sprouts from the formed gap when the bulk dipole coupling is pushed up further such as to overshadow the charge parameter, which is obviously different from what is found at the relativistic fixed points.

Contents

1. Introduction	1
2. Holographic implementation of various fermionic fixed points	2
3. Holographic non-relativistic fermion with bulk dipole coupling	6
3.1 Holographic setup	6
3.2 Numerical results	9
4. Conclusions	15

1. Introduction

Arising from the string theory, AdS/CFT correspondence has provided us with a new paradigm to study strongly coupled many body phenomena by relating them to a single or few body problem in the bulk classical gravitational backgrounds with one extra dimension. In applying AdS/CFT correspondence, there are two approaches which have been taken. One is the so called bottom-up approach, where the bulk setup is devised in a simple way but the microscopic understanding of dual field theory is generically lacking. The other is the so called top-down approach, where the whole setup can be embedded in the more sophisticated string theory or M theory such that the microscopic content of boundary field theory is well understood, although the system may not be realized in Nature. However, such a shortcoming is somehow mitigated by focusing judiciously on the IR physics, where it is believed that the same universal behaviors can be extracted from this sort of holographic duality for those realistic systems which may have different microscopic contents.

With this in mind, attempts to apply this holographic technique, with some success, have gone beyond high energy physics, especially to condensed matter physics in the recent years. Obviously, it is kind of win-win game to apply the holography to condensed matter physics. On the one hand, there exist many strong coupled systems in condensed matter physics, which are intractable by the conventional approaches. While AdS/CFT correspondence, as kind of strong/weak duality, can offer unprecedented insight into the dynamics of these systems. On the other hand, unlike other disciplines

such as high energy physics and cosmology, only with some tabletop experiments, does condensed matter physics allow one to cook up matter such that various vacuum states and phases can be created in the laboratory. With this available landscape of man-made multiverse to scan, it is highly possible for us to hit some universality classes extracted from the holography. In this sense, condensed matter physics may in turn provide us with the first experimental evidence for AdS/CFT correspondence. For a review of this exciting subject, please refer to [1, 2, 3, 4, 5].

In particular, partly triggered by the lack of a proper field theoretical framework to explain for the mysterious behaviors of existing non-Fermi liquids, endeavors have been made recently to study the spectral function of fermionic operators by holographically manipulating the bulk Dirac field which is minimally coupled to gravity and gauge fields, where the emergence of Fermi surface has been identified with a rich spectrum of non-Fermi liquid behaviors[6, 7, 8, 9, 10, 11]. Later on, inspired by the generic top-down models, the bottom-up dipole coupling has been added to the previous minimally coupled Dirac field and its effects on the fermionic correlator have been investigated, where a possible dynamical gap opens up when the dipole coupling is tuned to be large enough[12, 13, 14]¹. Generically, in the context of AdS/CFT correspondence, not only the modification of bulk dynamics, but also the change of boundary conditions can alter the boundary field theory. Actually, in the latter manner, the holographic non-relativistic fermionic fixed points have been implemented most recently by adding a Lorentz violating boundary term instead of the conventional Lorentz covariant one to the bulk minimally coupled Dirac action, where a holographic flat band is achieved[17].

Along this line, this paper is intended to insist on one of these novel non-relativistic fixed points and investigate how the fermionic correlator is modified when we turn on the bulk dipole coupling. In the next section, we shall provide a brief review of how both of the relativistic and non-relativistic fermionic fixed points are implemented by holography. In Section 3, after building up the holographic framework to extract the fermionic correlator at the non-relativistic fermionic fixed point, we shall present our numerical results for the relevant quantities associated with the fermionic correlator in the presence of bulk dipole coupling. Conclusions and discussions will be addressed in the end.

2. Holographic implementation of various fermionic fixed points

Start with the bulk action for a probe Dirac fermion with the mass m , charge q and

¹It is noteworthy that the impact of bulk dipole coupling on fermionic correlator has also been fully explored from the purely top-down construction in [15] and [16].

magnetic dipole coupling p

$$S_{bulk} = \int_{\mathcal{M}} d^4x \sqrt{-g} i \bar{\psi} \left[\frac{1}{2} (\overrightarrow{\mathcal{D}} - \overleftarrow{\mathcal{D}}) - m - ip \not{F} \right] \psi \quad (2.1)$$

in the following fixed background, i.e.,

$$ds^2 = r^2 [-f(r)(dt)^2 + (dx^1)^2 + (dx^2)^2] + \frac{1}{r^2} \frac{(dr)^2}{f(r)}, A_a = A_t(dt)_a. \quad (2.2)$$

Here $\bar{\psi} = \psi^\dagger \Gamma^t$, $\overrightarrow{\mathcal{D}} = (e_\mu)^a \Gamma^\mu [\partial_a + \frac{1}{4} [(\omega_{\rho\sigma})_a \Gamma^{\rho\sigma} - iq A_a]]$, and $\not{F} = \frac{1}{4} \Gamma^{\mu\nu} (e_\mu)^a (e_\nu)^b F_{ab}$, where $(e_\mu)^a$ form a set of orthogonal normal vector bases, and Gamma matrices satisfy $\{\Gamma^\mu, \Gamma^\nu\} = 2\eta^{\mu\nu}$ with the spin connection $(\omega_{\mu\nu})_a = (e_\mu)_b \nabla_a (e_\nu)^b$, $\Gamma^{\mu\nu} = \frac{1}{2} [\Gamma^\mu, \Gamma^\nu]$, and the field strength $F = dA$. In addition, the emblackening factor and gauge potential are given by

$$f = 1 - \frac{1 + Q^2}{r^3} + \frac{Q^2}{r^4}, A_t = g_F Q \left(1 - \frac{1}{r}\right), \quad (2.3)$$

which arises as the charged black hole solution to the equation of motion following from the bulk action for the gauge field coupled to AdS gravity with the gauge coupling g_F , i.e.,

$$S = \frac{1}{2\kappa^2} \int_{\mathcal{M}} d^4x \sqrt{-g} \left[R - \frac{6}{L^2} - \frac{L^2}{g_F^2} F_{\mu\nu} F^{\mu\nu} \right], \quad (2.4)$$

where L is the curvature radius, and has been set to unity along with the horizon radius. By holography, such a charged black hole places the probe fermion into the dual strongly coupled soup with the finite temperature and chemical potential as

$$T = \frac{3 - Q^2}{4\pi}, \mu = g_F q Q. \quad (2.5)$$

Now to have a well-defined variational principle for the Dirac action, a boundary term must be added. To see this, let us make the variation of bulk action, which gives rise to

$$\begin{aligned} \delta S_{bulk} = & i \int_{\mathcal{M}} d^4x \sqrt{-g} \left[\delta \bar{\psi} (\overrightarrow{\mathcal{D}} - m - ip \not{F}) \psi - \bar{\psi} (\overleftarrow{\mathcal{D}} + m + ip \not{F}) \delta \psi \right] \\ & + \frac{i}{2} \int_{\partial \mathcal{M}} d^3x \sqrt{-h} (\bar{\psi}_- \delta \psi_+ - \bar{\psi}_+ \delta \psi_- + \delta \bar{\psi}_+ \psi_- - \delta \bar{\psi}_- \psi_+) \end{aligned} \quad (2.6)$$

where $h = \frac{g}{g_{rr}}$ is the determinant of induced metric on the boundary, and $\psi_\pm = \frac{1}{2}(1 \pm \Gamma^r)\psi$. Note that the bulk Dirac equation

$$(\overrightarrow{\mathcal{D}} - m - ip \not{F})\psi = 0 \quad (2.7)$$

is first order. So it is not allowable to fix all components of ψ , namely both of ψ_+ and ψ_- . Instead we must somehow fix simply half of the components of ψ , which can actually be implemented by adding a boundary term. Moreover, it turns out that the variational principle can be achieved by adding a number of different boundary terms, depending on the specific value of the mass parameter m^2 .

The conventional boundary term chosen to be added is the Lorentz covariant one, i.e.,

$$S_{bdy} = \frac{i}{2} \int_{\partial\mathcal{M}} \sqrt{-h} \bar{\psi} \psi = \frac{i}{2} \int_{\partial\mathcal{M}} \sqrt{-h} (\bar{\psi}_- \psi_+ + \bar{\psi}_+ \psi_-), \quad (2.8)$$

whereby the variation of the full on-shell action is given by

$$\delta S_{bulk} + \delta S_{bdy} = i \int_{\partial\mathcal{M}} d^3x \sqrt{-h} (\bar{\psi}_- \delta\psi_+ + \delta\bar{\psi}_+ \psi_-), \quad (2.9)$$

which indeed vanishes if and only if the Dirichlet boundary condition is imposed on ψ_+ . This sort of choice of boundary condition is usually referred to as the standard quantization for the Dirac field. As a result, the dual boundary field theory is a Lorentz covariant CFT where loosely speaking ψ_+ plays a role of fermionic source, and the dual operator is given by ψ_- with dimension

$$\Delta[\psi_-] = \frac{3}{2} + m. \quad (2.10)$$

When the mass parameter is tuned into the window $0 \leq m < \frac{1}{2}$, we can have other boundary conditions to choose. The first one is the so called alternative quantization, which can be implemented simply by adding the boundary term with opposite sign, i.e.,

$$S_{bdy} = -\frac{i}{2} \int_{\partial\mathcal{M}} \sqrt{-h} \bar{\psi} \psi = -\frac{i}{2} \int_{\partial\mathcal{M}} \sqrt{-h} (\bar{\psi}_- \psi_+ + \bar{\psi}_+ \psi_-). \quad (2.11)$$

This now results in a well defined variational principle if and only if one imposes the Dirichlet boundary condition on ψ_- . The dual boundary field theory is still a Lorentz covariant CFT with the fermionic source and dual operator interchanged. The dimension of operator is thus given by

$$\Delta[\psi_+] = \frac{3}{2} - m. \quad (2.12)$$

We have other boundary conditions to choose if we are not only interested in the Lorentz covariant boundary field theory. In particular, as shown in [17], a non-relativistic

²For simplicity but without loss of generality, we shall focus on the case of $m \geq 0$ in what follows.

fermionic fixed point can be implemented by adding the following Lorentz violating boundary term, i.e.,

$$S_{bdy} = \frac{1}{2} \int_{\partial\mathcal{M}} d^3x \sqrt{-h} \bar{\psi} \Gamma^1 \Gamma^2 \psi. \quad (2.13)$$

To see explicitly what both of the corresponding fermionic source and dual operator look like, we would like to firstly choose our Gamma matrices once and for all as follows

$$\Gamma^r = \begin{pmatrix} -\sigma^3 & 0 \\ 0 & -\sigma^3 \end{pmatrix}, \quad \Gamma^t = \begin{pmatrix} i\sigma^1 & 0 \\ 0 & i\sigma^1 \end{pmatrix}, \quad \Gamma^1 = \begin{pmatrix} -\sigma^2 & 0 \\ 0 & \sigma^2 \end{pmatrix}, \quad \Gamma^2 = \begin{pmatrix} 0 & -i\sigma^2 \\ i\sigma^2 & 0 \end{pmatrix}, \quad (2.14)$$

where σ^i are Pauli matrices³. With this kind of choice of Gamma matrices, we can express ψ_+ and ψ_- as

$$\psi_+ = (-h)^{-\frac{1}{4}} \begin{pmatrix} 0 \\ z_1 \\ 0 \\ z_2 \end{pmatrix}, \quad \psi_- = (-h)^{-\frac{1}{4}} \begin{pmatrix} y_1 \\ 0 \\ y_2 \\ 0 \end{pmatrix}. \quad (2.15)$$

Hereby the variation of bulk on-shell action can be massaged as

$$\delta S_{bulk} = -\frac{1}{2} \int_{\partial\mathcal{M}} d^3x (\delta z_1^\dagger y_1 + \delta z_2^\dagger y_2 - \delta y_1^\dagger z_1 - \delta y_2^\dagger z_2 - z_1^\dagger \delta y_1 - z_2^\dagger \delta y_2 + y_1^\dagger \delta z_1 + y_2^\dagger \delta z_2). \quad (2.16)$$

On the other hand, by $\psi = \psi_+ + \psi_-$, the Lorentz violating boundary term can be casted into

$$S_{bdy} = -\frac{1}{2} \int_{\partial\mathcal{M}} d^3x (z_2^\dagger y_1 + y_2^\dagger z_1 + z_1^\dagger y_2 + y_1^\dagger z_2). \quad (2.17)$$

Whence the variation of full on-shell action is given by

$$\begin{aligned} \delta S_{bulk} + \delta S_{bdy} &= -\frac{1}{2} \int_{\partial\mathcal{M}} d^3x [\delta(z_1^\dagger + z_2^\dagger)(y_1 + y_2) + \delta(y_1^\dagger - y_2^\dagger)(z_2 - z_1) \\ &\quad + (z_2^\dagger - z_1^\dagger)\delta(y_1 - y_2) + (y_1^\dagger + y_2^\dagger)\delta(z_1 + z_2)] \\ &= -\int_{\partial\mathcal{M}} d^3x (\delta Z_1^\dagger Y_1 + Z_2^\dagger \delta Y_2 + Y_1^\dagger \delta Z_1 + \delta Y_2^\dagger Z_2), \end{aligned} \quad (2.18)$$

where we have defined $(Y_1, Y_2) = \frac{1}{\sqrt{2}}(y_1 + y_2, y_1 - y_2)$, and $(Z_1, Z_2) = \frac{1}{\sqrt{2}}(z_1 + z_2, z_2 - z_1)$. Hence the corresponding fermionic source and dual operator are somehow given by (Z_1, Y_2) and (Y_1, Z_2) respectively, and the dimension of operator reads

$$\Delta[Y_1] = \frac{3}{2} + m, \quad \Delta[Z_2] = \frac{3}{2} - m. \quad (2.19)$$

³Note that our choice of Gamma matrices is different from that in [17]. We are believed that our choice is more suitable for performing the practical calculation, which can be seen later on.

Regarding other possible choices of boundary conditions and how they are related to one another through the Wilsonian RG flow by the double trace deformation, please refer to [17, 18]. In the subsequent section, we will focus only on the above non-relativistic fixed point, to extract the boundary fermionic correlator from the bulk dynamics and see how the magnetic dipole coupling affects the fermionic correlator by numerical calculation.

3. Holographic non-relativistic fermion with bulk dipole coupling

3.1 Holographic setup

Generically the relevant information regarding the fermionic system can be read out of its single particle fermionic correlator, namely the retarded Green function G_R . For example, the spectral function $A(\omega, k)$, which can be measured experimentally by Angle Resolved Photoemission Spectroscopy(ARPES), is given by the imaginary part of $\text{Tr}G_R$. Now we shall show how such a retarded Green function can be obtained holographically.

To proceed, we would like to start with the Dirac equation (2.7) in a more general static background, i.e.,

$$ds^2 = -g_{tt}(r)dt^2 + g_{rr}(r)dr^2 + g_{xx}(r)[(dx^1)^2 + (dx^2)^2], A_a = A_t(r)(dt)_a. \quad (3.1)$$

Then we choose the orthogonal normal vector bases as follows

$$(e_t)^a = \frac{1}{\sqrt{g_{tt}}}(\frac{\partial}{\partial t})^a, (e_i)^a = \frac{1}{\sqrt{g_{xx}}}(\frac{\partial}{\partial x^i})^a, (e_r)^a = \frac{1}{\sqrt{g_{rr}}}(\frac{\partial}{\partial r})^a, \quad (3.2)$$

from which the non-vanishing components of spin connection can be obtained as

$$(\omega_{tr})_a = -(\omega_{rt})_a = -\frac{\partial_r \sqrt{g_{tt}}}{\sqrt{g_{rr}}}(dt)_a, (\omega_{ir})_a = -(\omega_{ri})_a = \frac{\partial_r \sqrt{g_{xx}}}{\sqrt{g_{rr}}}(dx^i)_a. \quad (3.3)$$

Next let $\psi = (-h)^{-\frac{1}{4}}\varphi$, then the bulk Dirac equation can be expressed as

$$\frac{\Gamma^r \partial_r \varphi}{\sqrt{g_{rr}}} + \frac{\Gamma^t (\partial_t - iqA_t) \varphi}{\sqrt{g_{tt}}} + \frac{\Gamma^i \partial_i \varphi}{\sqrt{g_{xx}}} - m\varphi - \frac{ip\Gamma^{rt} \partial_r A_t}{2\sqrt{g_{tt}g_{rr}}}\varphi = 0. \quad (3.4)$$

By the rotation symmetry in the spatial directions, without loss of generality, we shall let $\varphi = e^{-i\omega t + ikx^1} \tilde{\varphi}$, thus the Dirac equation reduces to

$$\frac{\sqrt{g_{xx}}}{\sqrt{g_{rr}}}(\Gamma^r \partial_r - m\sqrt{g_{rr}} - \frac{ip\Gamma^{rt} \partial_r A_t}{2\sqrt{g_{tt}}})\tilde{\varphi} + (-iu\Gamma^t + ik\Gamma^1)\tilde{\varphi} = 0, \quad (3.5)$$

where

$$u = \frac{\sqrt{g_{xx}}}{\sqrt{g_{tt}}}(\omega + qA_t). \quad (3.6)$$

Set $\tilde{\varphi} = \begin{pmatrix} \tilde{\varphi}_1 \\ \tilde{\varphi}_2 \end{pmatrix}$, then with our representation of Gamma matrices, the equation of motion can be further simplified as

$$\frac{\sqrt{g_{xx}}}{\sqrt{g_{rr}}}(\partial_r + m\sqrt{g_{rr}}\sigma_3)\tilde{\varphi}_I = \left[i\sigma_2 u + [(-1)^I k - \frac{p\sqrt{g_{xx}}\partial_r A_t}{\sqrt{g_{tt}g_{rr}}}] \sigma_1 \right] \tilde{\varphi}_I, \quad (3.7)$$

with $I = 1, 2$. Moreover, by $\tilde{\varphi}_I = \begin{pmatrix} \tilde{y}_I \\ \tilde{z}_I \end{pmatrix}$, the above equation of motion gives rise to the following flow equation, i.e.,

$$\frac{\sqrt{g_{xx}}}{\sqrt{g_{rr}}}\partial_r \xi_I = -2m\sqrt{g_{xx}}\xi_I + \left[u - \frac{p\sqrt{g_{xx}}\partial_r A_t}{\sqrt{g_{tt}g_{rr}}} + (-1)^I k \right] + \left[u + \frac{p\sqrt{g_{xx}}\partial_r A_t}{\sqrt{g_{tt}g_{rr}}} - (-1)^I k \right] \xi_I^2 \quad (3.8)$$

where $\xi_I = \frac{\tilde{y}_I}{\tilde{z}_I}$. Now plug the particular background (2.2) into the above equations, we end up with

$$(r^2\sqrt{f}\partial_r + rm\sigma_3)\tilde{\varphi}_I = \left[\frac{i\sigma_2}{\sqrt{f}}\left[\omega + qg_F Q\left(1 - \frac{1}{r}\right)\right] + [(-1)^I k - \frac{pg_F Q}{r}] \right] \tilde{\varphi}_I \quad (3.9)$$

for the equation of motion, and

$$r^2\sqrt{f}\partial_r \xi_I = -2mr\xi_I + [v_- + (-1)^I k] + [v_+ - (-1)^I k] \xi_I^2 \quad (3.10)$$

for the flow equation, where

$$v_{\pm} = \frac{1}{\sqrt{f}}\left[\omega + qg_F Q\left(1 - \frac{1}{r}\right)\right] \pm \frac{pg_F Q}{r}. \quad (3.11)$$

Whence near the boundary, namely when r goes to the infinity, $\tilde{\varphi}_I$ behave in the following way, i.e.,

$$\tilde{\varphi}_I \rightarrow c_I r^m \begin{pmatrix} 0 \\ 1 \end{pmatrix} + d_I r^{-m} \begin{pmatrix} 1 \\ 0 \end{pmatrix}. \quad (3.12)$$

The ratio $G_I = \frac{d_I}{c_I}$ can be fixed by imposing the in-falling boundary condition for $\tilde{\varphi}$ at the horizon, where $\tilde{\varphi}_I$ behave as

$$\tilde{\varphi}_I \propto \begin{pmatrix} i \\ 1 \end{pmatrix} e^{-i\omega r_*} \quad (3.13)$$

with $r_* = \int \frac{dr}{r^2 f}$. Alternatively, this ratio can also be obtained in a more convenient way as

$$G_I = \lim_{r \rightarrow \infty} r^{2m} \xi_I, \quad (3.14)$$

by solving the flow equation (3.10) with the boundary condition at the horizon

$$\xi_I = i. \quad (3.15)$$

Then by the recipe of AdS/CFT, it follows from the variation of on-shell action (2.18) that at the non-relativistic fixed point the retarded fermionic Green correlator can be extracted from the following relation, i.e.,

$$\begin{pmatrix} D_1 \\ C_2 \end{pmatrix} = G_R \begin{pmatrix} C_1 \\ D_2 \end{pmatrix} = \begin{pmatrix} \alpha & \beta \\ \gamma & \eta \end{pmatrix} \begin{pmatrix} C_1 \\ D_2 \end{pmatrix} \quad (3.16)$$

with $(D_1, D_2) = \frac{1}{\sqrt{2}}(d_1 + d_2, d_1 - d_2)$ and $(C_1, C_2) = \frac{1}{\sqrt{2}}(c_1 + c_2, c_2 - c_1)$. To be more precise, from such a relation, we have

$$\begin{aligned} \frac{\alpha}{G_1} + \beta &= 1, & \frac{\alpha}{G_2} - \beta &= 1, \\ \gamma + \eta G_1 &= -1, & \gamma - \eta G_2 &= 1, \end{aligned} \quad (3.17)$$

which gives G_R in terms of G_I as⁴

$$G_R = \begin{pmatrix} \frac{2G_1 G_2}{G_1 + G_2} & \frac{G_1 - G_2}{G_1 + G_2} \\ \frac{G_1 - G_2}{G_1 + G_2} & \frac{-2}{G_1 + G_2} \end{pmatrix}. \quad (3.18)$$

Consequently, $\det(G_R) = -1$, and the trace along with the eigenvalues of G_R can be worked out as

$$\lambda_{\pm} = \frac{G_1 G_2 - 1 \pm \sqrt{1 + G_1^2 + G_2^2 + G_1^2 G_2^2}}{G_1 + G_2} \quad (3.19)$$

$$\text{Tr} G_R = \lambda_+ + \lambda_- = \frac{2G_1 G_2 - 2}{G_1 + G_2}. \quad (3.20)$$

It follows from the flow equation (3.10) that G_1 and G_2 are related to each other as

$$G_2(\omega, k) = G_1(\omega, -k). \quad (3.21)$$

⁴It is noteworthy that G_I are simply the components of diagonal retarded Green function in the standard quantization. An intriguing question is how to understand (3.18) directly from the RG flow induced by the double trace deformation.

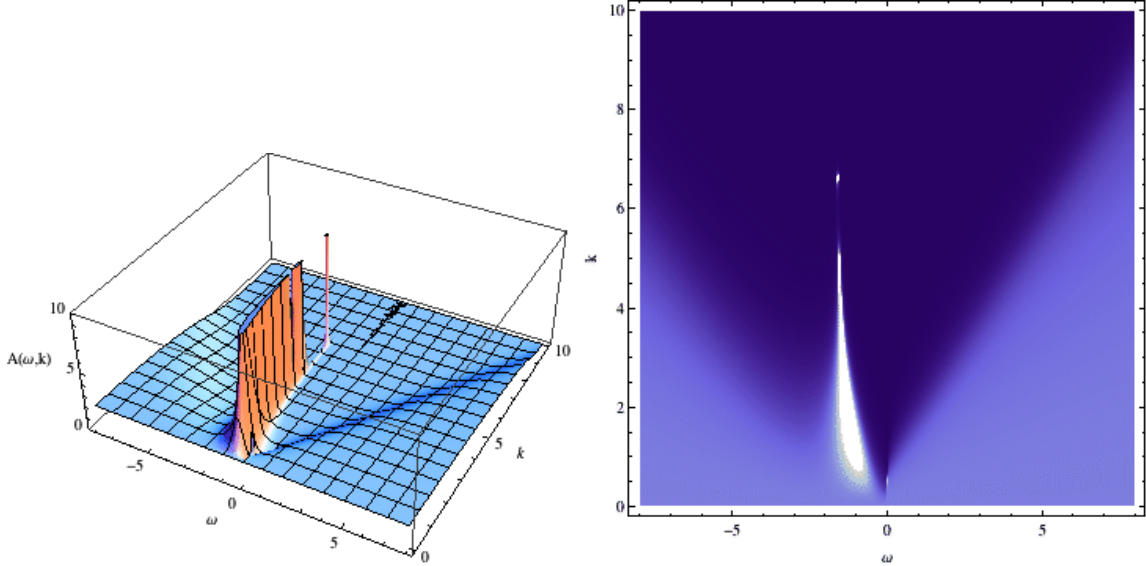


Figure 1: The 3d and density plots of spectral function for the case of $q = 1$ and $p = 0$.

Therefore both of the trace and eigenvalues of our retarded Green function are invariant under the transformation $k \rightarrow -k$ as it should be, guaranteed by the rotation symmetry mentioned above. In addition, by the flow equation, we also have

$$G_1(\omega, k; g_F) = -G_2^*(-\omega, k; -g_F), \quad (3.22)$$

or equivalently

$$G_1(\omega, k; q, p) = -G_2^*(-\omega, k; -q, -p). \quad (3.23)$$

To make our life easier, in what follows, we will set $g_F = 1$ and work exclusively with the case of $m = 0$, where the flow equation further implies

$$G_1(\omega, k; p) = -\frac{1}{G_2(\omega, k; -p)}. \quad (3.24)$$

So it is essentially enough to restrict ourselves to non-negative k , q and p .

3.2 Numerical results

In the following numerical calculations, we shall focus exclusively on the probe fermion in the zero temperature soup, which can be achieved by setting $Q = \sqrt{3}$. Then the chemical potential is given by $\mu = \sqrt{3}q$.

We start by fixing $q = 1$ but varying p . The corresponding numerical results are plotted in Figures 1, 2, 3, and 4, where the 3d and density plots are drawn for the spectral function on the left and right respectively. First, albeit with the different choice

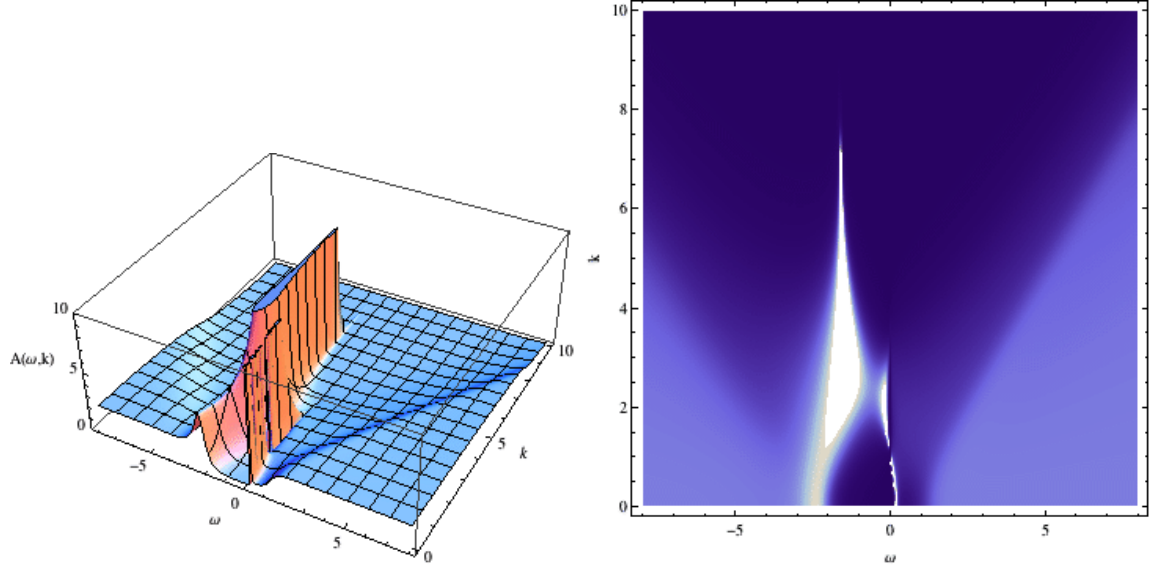


Figure 2: The 3d and density plots of spectral function for the case of $q = 1$ and $p = 2$.

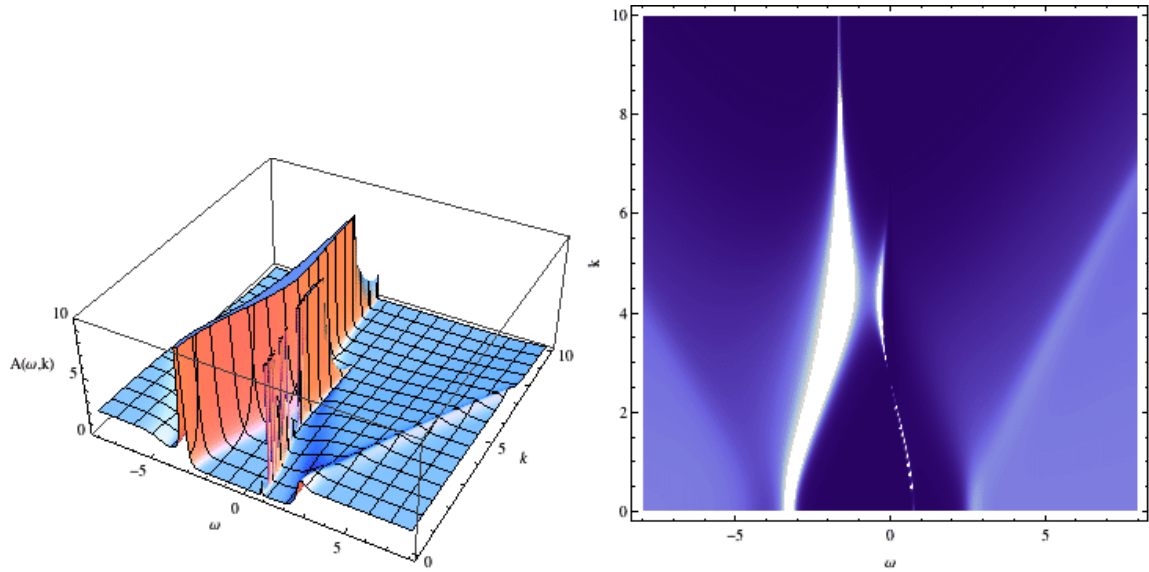


Figure 3: The 3d and density plots of spectral function for the case of $q = 1$ and $p = 4$.

of Gamma matrices the result presented in Figure 1 is consistent with that obtained in [17], where instead of the spectral function, $\text{Im}\lambda_+$ and $\text{Im}\lambda_-$ are plotted individually⁵.

⁵As pointed out to us by Robert Leigh, $\text{Im}\lambda_+$ and $\text{Im}\lambda_-$ can also be measured by the so called spin polarized ARPES. The reason why we work only with the spectral function lies in the fact that unlike the trace of retarded Green function the expression for two eigenvalues generically involves the square root, as shown in (3.19). Such a square root makes it less easy to separate these two eigenvalues by our

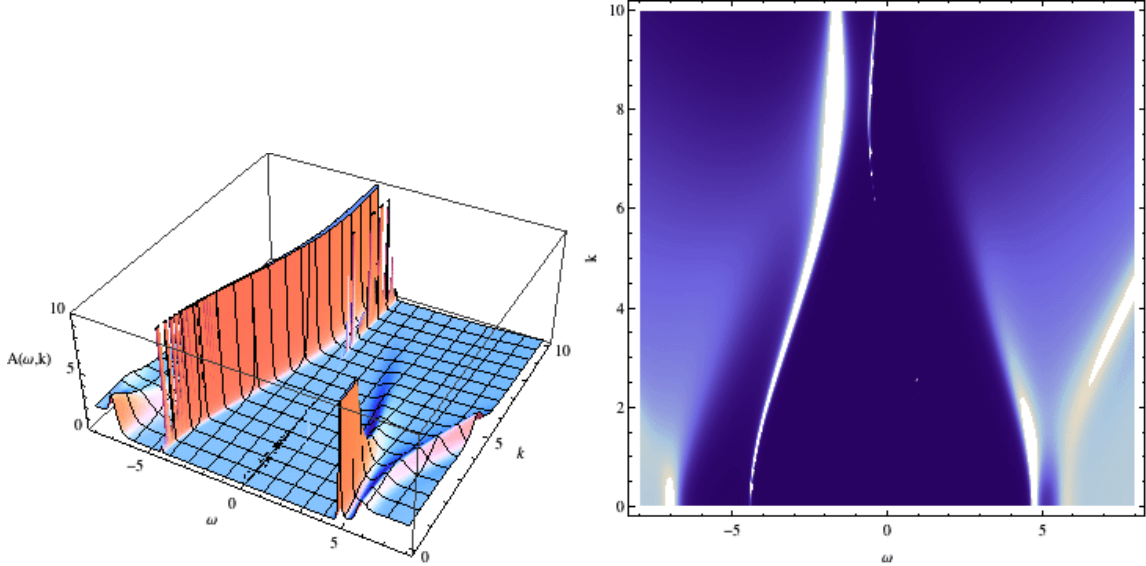


Figure 4: The 3d and density plots of spectral function for the case of $q = 1$ and $p = 8$.

q=1	p=0	p=2	p=4	p=8
k_F	No	1.08188	2.63542	4.87894

Table 1: The Fermi momentum for the case of $q = 1$.

This can be regarded as sort of consistency check on our numerics. Second, with the finite chemical potential the infinite flat band get mildly dispersed. In the large momentum limit, the band becomes asymptotically flat. This is reasonable as at large momenta the corresponding modes sit outside of the light cone and can not decay. Furthermore, as one goes to the large momentum limit, the flat band is always shifted to $\omega = -\sqrt{3}$, independent of the specific value of p , which arises because the frequency is measured with respect to the chemical potential. But the larger becomes the value of p , the larger becomes the momentum at which the peak of flat band tends to be sharp, which is somehow related to something more interesting occurring in the region of small momenta. The infinite band, which is destroyed or depleted from zero momentum up to the momentum of the order of the finite chemical potential by colliding our probe fermion with the relativistic soup, is gradually recovered to extend down to zero momentum as one pushes the bulk dipole coupling up. In particular, at the momenta lower than the value of p the flat band disperses the other way than it does at large momenta. This implies that it costs more energy to excite small momentum modes

numerical calculations. The only exception is the case of $m = 0$ and $p = 0$, where the two eigenvalues can be explicitly massaged as $\lambda_+ = \frac{G_1-1}{G_1+1}$ and $\lambda_- = \frac{1+G_1}{1-G_1}$ by using (3.24).

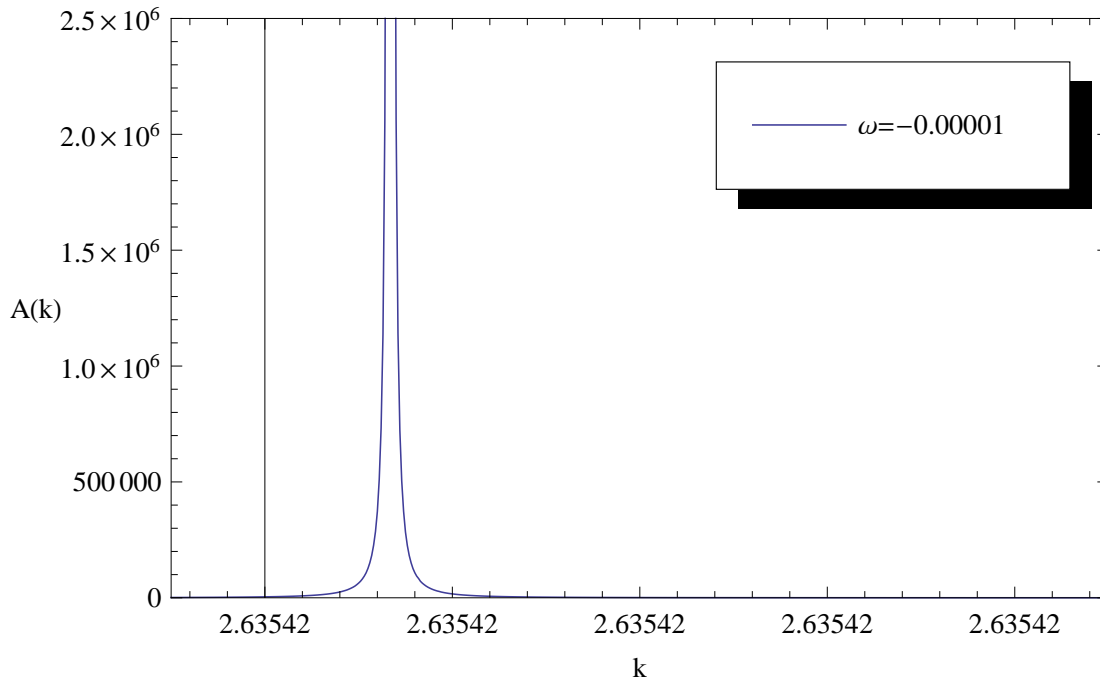


Figure 5: The Fermi momentum can be fixed to the 5th digit as $k_F = 2.63542$ by taking $\omega = -0.00001$ for the case of $q = 1$ and $p = 4$.

than intermediate momentum modes, which is also consistent with the phenomenon that the peak of flat band becomes sharper and sharper at small momenta as p is increased. Moreover, as shown in Figure 4, some other gap states, which are nearly flat finite bands, are generated at small momenta when the value of p is large enough.

On the other hand, as p increases, the Fermi surface starts to show up at some point with the Fermi momentum increasing. To be more precise, as demonstrated in Figure 5, we can identify the location of Fermi surface to the 5th digit using the fact that the location of peak approaches the Fermi surface k_F in the limit $\omega \rightarrow 0$. The corresponding results are listed in Table 1⁶. It is noteworthy that such a situation is different from what is happening to the relativistic fixed points, where the Fermi surface disappears and instead the gap forms when the bulk dipole coupling is large enough[12].

Now let us move on to the case of $q = 2$. As shown in Figure 6, 7, 8, and 9, some new features come in, namely, the original Fermi surface disappears, accompanied by a gap opening up at negative ω as one increases the dipole coupling p from zero. But

⁶Note that in Figure 4 the apparent disappearance of the peak around $\omega = 0$ is sort of numerical artifact. It arises because the peak becomes sharper as one approaches $\omega = 0$.

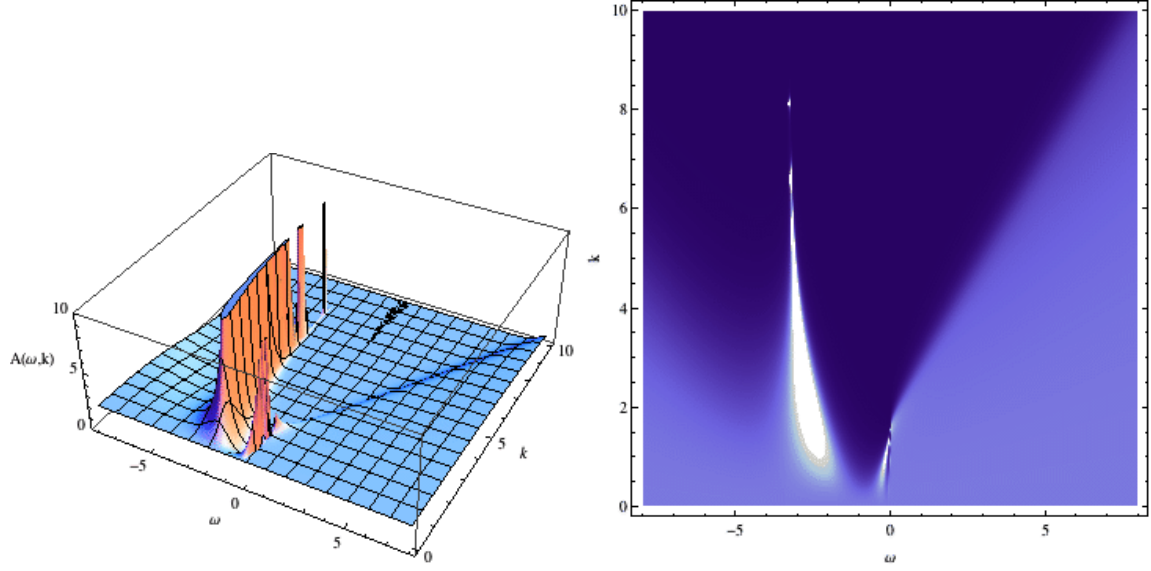


Figure 6: The 3d and density plots of spectral function for the case of $q = 2$ and $p = 0$, where the Fermi surface shows up with the Fermi momentum $k_F = 1.53521$.

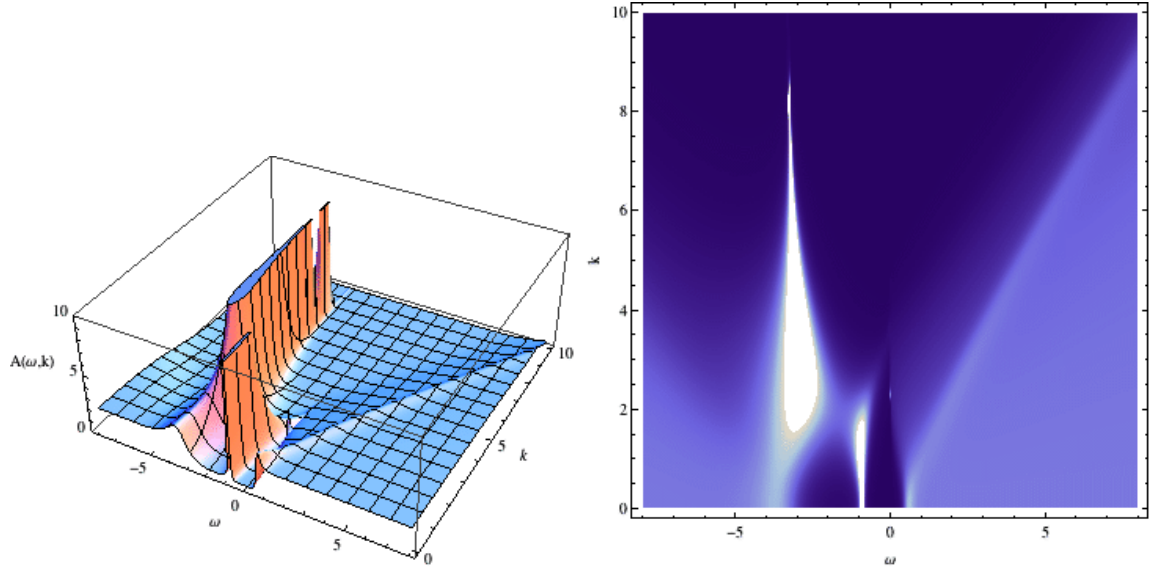


Figure 7: The 3d and density plots of spectral function for the case of $q = 2$ and $p = 2$, where the Fermi surface disappears and a flat gap sits at $\omega = -0.85$.

as p is increased further, the gap gets bent gradually towards $\omega = 0$. Finally the gap closes up, followed by the sprouting of a new Fermi surface. This suggests that there is some kind of competition between the charge q and the bulk dipole coupling p . Each of them prefers to create their own Fermi surfaces. The gap exists at the parameter

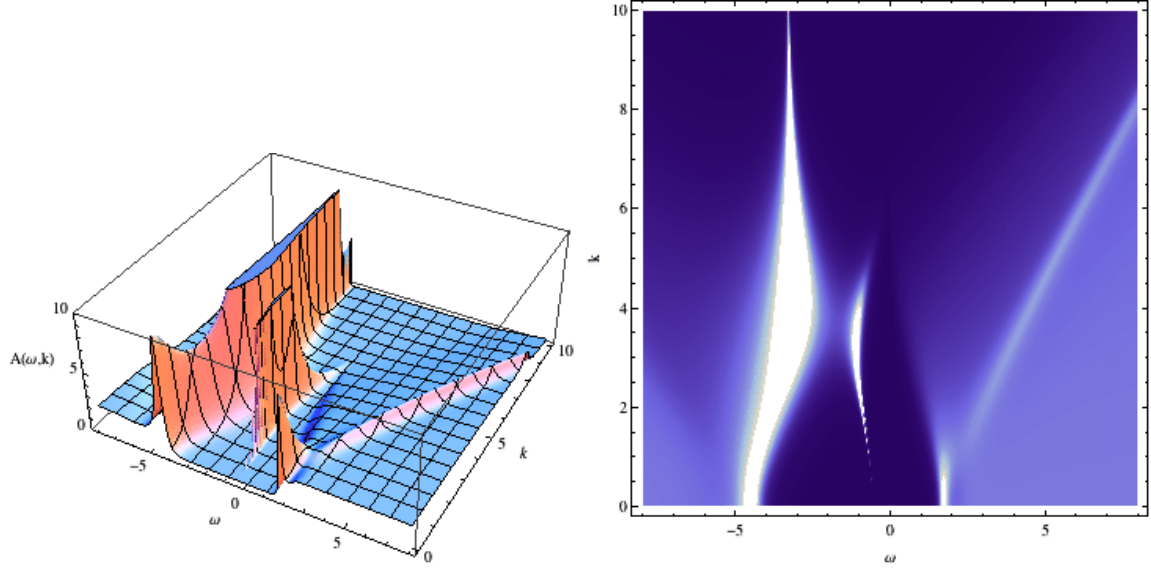


Figure 8: The 3d and density plots of spectral function for the case of $q = 2$ and $p = 4$, where the gap bends towards $\omega = 0$ with the gap energy $\omega = -0.56$ for the zero momentum mode.

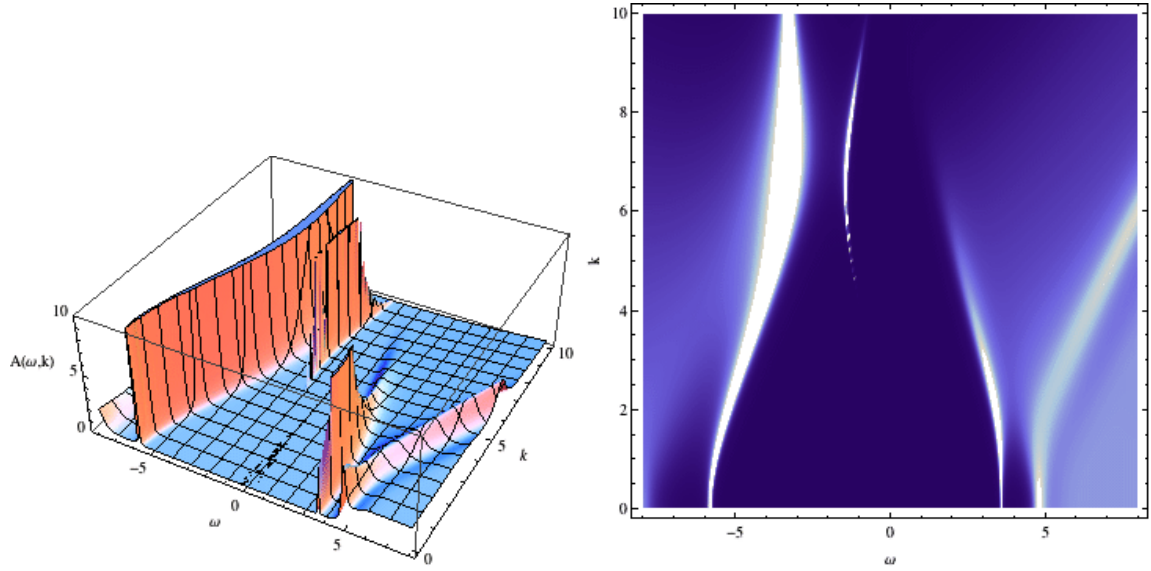


Figure 9: The 3d and density plots of spectral function for the case of $q = 2$ and $p = 8$, where the bent gap sprouts a new Fermi surface with the Fermi momentum $k_F = 1.20996$.

place where they counterbalance each other. Such a pattern can be checked to persist for other larger charge cases. Finally, we would like to emphasize that such a rebirth of Fermi surface from the generated gap like a phoenix is never occurring at the relativistic

fixed points, where instead the gap is generically enlarged as the bulk dipole coupling is increased[13].

4. Conclusions

We have worked with one of the recently discovered non-relativistic fermionic fixed points and investigated how the corresponding spectral function is modified by the bulk dipole term numerically. As a result, although the infinite flat band is robust against the bulk dipole coupling as well as chemical potential, the bulk dipole coupling modifies the flat band in particular at the momenta lower than the value of bulk dipole coupling, bending the band towards more negative frequencies. More remarkably, it is shown that a new Fermi surface emerges from the gradually disappearing gap as the bulk dipole coupling starts to outweigh the charge parameter, which is totally different from what is happening at the relativistic fixed points. It is definitely worthwhile to identify such features by scanning the realistic condensed matter systems and see what kind of role the bulk dipole coupling mimics there.

We conclude with various directions worthy of further investigation in the near future. First, although for the cases of $m \neq 0$ the retarded Green function is expected to exhibit the qualitatively similar behaviors as the massless story we have told above, it is interesting to investigate how some specific features of retarded Green function like the location of Fermi momentum depend quantitatively on the mass m . Second, it is intriguing to heat up our system to a finite temperature by considering the charged AdS black hole away from the extremality to see which features are smoothed out by such a finite temperature while which features can persist against the temperature. Last but not least, as is well known, the low energy behaviors around the Fermi surface are controlled by the $AdS_2 \times R^2$ region near the horizon for the relativistic fixed points. On the other hand, only in how to massage the boundary data does the difference lie between the non-relativistic and relativistic fixed points. The bulk dynamics is the same for all of these fixed points. So it is expected that at the non-relativistic fixed points the low energy behaviors around the Fermi surface are also determined by the emergent IR CFT associated with the $AdS_2 \times R^2$ region somehow. In particular, it is highly desirable to have an analytic understanding of the low energy behaviors around the Fermi surface at the non-relativistic fixed points by performing the rigmarole of matching calculation. We expect to explore these issues elsewhere.

Acknowledgements

We would like to thank David Tong for his insightful and illuminating correspondence

during the whole course of this project. WJL is grateful to Sijie Gao for his everlasting encouragement and stimulating discussions. He is also indebted to Xiaomei Kuang for her help to run part of our Mathematica programs in her personal computer and Jianpin Wu for his sharing the experience in identifying the Fermi surface numerically. HZ is grateful to John McGreevy during PASCOS 2011 in Cambridge and Robert Leigh during the 41th Summer Institute in Paris for their valuable explanations of their independent works, which are relevant to our project. HZ is also indebted to Rene Meyer and Zhi Wang for helpful discussions. In addition, he appreciates Ioannis Iatrakis and Matti Jarvinen for their very help with our Mathematica codes. He also acknowledges the Simons Summer Workshop in Mathematics and Physics 2011 in Stony Brook for the fantastic hospitality during the initial stage of this project. WJL was supported in part by the NSFC under grant No.10605006 together with 10975016 and by the Fundamental Research Funds for the Central Universities. HZ was partially supported by a European Union grant FP7-REGPOT-2008-1-CreteHEPCosmo-228644. This research was also supported in part by the Project of Knowledge Innovation Program of Chinese Academy of Sciences, Grant No.KJCX2.YW.W10.

References

- [1] S. A. Hartnoll, *Class. Quant. Grav.* 26, 224002(2009)[arXiv:0903.3246[hep-th]].
- [2] C. P. Herzog, *J. Phys. A*42, 343001(2009)[arXiv:0904.1975[hep-th]].
- [3] J. McGreevy, *Adv. High Energy Phys.*, 723105(2010)[arXiv:0909.0518[hep-th]].
- [4] G. T. Horowitz, arXiv:1002.1722[hep-th].
- [5] S. Sachdev, arXiv:1002.2947[hep-th].
- [6] S. S. Lee, *Phys. Rev. D*79, 086006(2009)[arXiv:0809.3402[hep-th]].
- [7] H. Liu, J. McGreevy, and D. Vegh, *Phys. Rev. D*83, 065029(2011)[arXiv:0903.2477[hep-th]].
- [8] M. Cubrovic, J. Zaanen, and K. Schalm, *Science* 325, 439(2009)[0904.1993[hep-th]].
- [9] T. Faulkner, H. Liu, J. McGreevy, and D. Vegh, arXiv:1003.1728[hep-th].
- [10] T. Faulkner, N. Iqbal, H. Liu, J. McGreevy, and D. Vegh, arXiv:1101.0597[hep-th].
- [11] N. Iqbal, H. Liu, and M. Mezei, arXiv:1110.3814[hep-th].
- [12] M. Edalati, R. Leigh, and P. W. Phillips, *Phys. Rev. Lett.*106, 091602(2011)[arXiv:1010.3238[hep-th]].

- [13] M. Edalati, R. Leigh, K. W. Lo, and P. W. Phillips, Phys. Rev. D83, 046012(2011)[arXiv:1012.3751[hep-th]].
- [14] D. Guarrera and J. McGreevy, arXiv:1102.3908[hep-th].
- [15] J. Gauntlett, J. Sonner, and D. Waldram, arXiv:1106.4694[hep-th].
- [16] J. Gauntlett, J. Sonner, and D. Waldram, arXiv:1108.1205[hep-th].
- [17] J. N. Laia and D. Tong, arXiv:1108.1381[hep-th].
- [18] J. N. Laia and D. Tong, arXiv:1108.2216[hep-th].